Ecological Complexity 26 (2016) 68–78

Contents lists available at ScienceDirect

Ecological Complexity

journal homepage: www.elsevier.com/locate/ecocom

Original Research Article

Network based early warning indicators of vegetation changes in a land–atmosphere model

Z. Yin [a,*], S.C. Dekker [b], M. Rietkerk [b], B.J.J.M. van den Hurk [a,c], H.A. Dijkstra [a]

[a] Institute for Marine and Atmospheric Research Utrecht, Utrecht University, Utrecht, The Netherlands
[b] Copernicus Institute of Sustainable Development, Utrecht University, Utrecht, The Netherlands
[c] Royal Netherlands Meteorological Institute, De Bilt, The Netherlands

ARTICLE INFO

Article history:
Received 2 October 2015
Received in revised form 3 February 2016
Accepted 26 February 2016
Available online 8 April 2016

Keywords:
Abrupt transition
Early warning signals
Network based indicator
Tipping point
Critical slowing down
Land–atmosphere model

ABSTRACT

Numerous model studies demonstrate that ecosystems might not shift smoothly with a gradual change in resource concentration. At specific points, vegetation can suddenly shift from one stable state to another. To predict such undesirable shifts, statistical indicators are proposed for early warning prediction. These so-called classical indicators can address whether vegetation state is moving towards the tipping point of an abrupt transition, however when the transition will occur is hard to predict. Recent studies suggest that complex network based indicators can improve early warning signals of abrupt transitions in complex dynamic systems. In this study, both classical and network based indicators are tested in a coupled land–atmosphere ecological model in which a scale-dependent hydrology-infiltration feedback and a large scale vegetation–precipitation feedback are represented. Multiple biomass equilibria are found in the model and abrupt transitions can occur when rainfall efficiency is decreased. Interaction network based indicators of these transitions are compared with classical indicators, such as the lag-1 autocorrelation and Moran's coefficient, with particular focus on the transition associated with desertification. Two criteria are used to evaluate the quality of these early warning indicators and several high quality network based indicators are identified.

1. Introduction

Ecosystems do not necessarily shift gradually with changes in the amount of resources (Scheffer et al., 2001; Ripple and Beschta, 2006; Móréh et al., 2009; Claussen et al., 2013; Dekker, 2013). Observed patterns strongly suggest that multiple equilibria exist under similar climate regimes (Hirota et al., 2011; Staver et al., 2011b; Scheffer et al., 2012), which implies that ecosystems may shift from one stable state to another (Rietkerk et al., 2004; Hirota et al., 2011). More importantly, most of these transitions are subcritical as the shift is irreversible (Scheffer et al., 2009; Kéfi et al., 2013). Such critical transitions may lead to catastrophic changes of the landscape (Staver et al., 2011a) and result in regular vegetation patterns (Rietkerk et al., 2004), which in turn strongly affects local climate through biophysical and biochemical feedbacks (Bonan, 2008; Seneviratne et al., 2010; Dekker et al., 2007).

To anticipate to potential catastrophic transition of ecosystems, numerous studies have tried to find early warning indicators of the transition to desertification (Rietkerk et al., 2004; Kéfi et al., 2007a; Scheffer et al., 2009; Dakos et al., 2008). The phenomenon of 'critical slowing down', expressing that the recovery rate of the system to perturbations decreases near such a transition, has lead to useful early warning indicators, such as the lag-1 autocorrelation (van Nes and Scheffer, 2007; Scheffer et al., 2009). Also indicators based on the changes in spatial correlation of vegetation patterns have been developed (Dakos et al., 2010). In general, however, these classical indicators show only irregular monotonic behaviour and it is difficult to determine how close the system is to transition and when to give an alarm. Ideally, one likes to have the availability of indicators which give a sharp peak just before the transition.

Indicators based on complex interaction networks were shown to have this desired 'peaky' property when applied to a highly conceptual ecological model, the local positive feedback model (Tirabassi et al., 2014). Although the network based indicators have a higher quality factor, for this model also the classical indicators perform well regarding the desertification transition. A more

* Corresponding author.
E-mail address: zun.yin@foxmail.com (Z. Yin).

http://dx.doi.org/10.1016/j.ecocom.2016.02.004
1476-945X/

challenging test of the capabilities of network based indicators is the scale-dependent feedback model suggested in Rietkerk et al. (2002). For this model, two classical indicators (lag-1 autocorrelation and Moran's coefficient, see Section 2.2) show unexpected trends when approaching the critical transition (Dakos et al., 2011).

As was indicated in Dijkstra (2011), the structure of the multiple equilibria in a scale-dependent feedback model is complicated because of the appearance of a multitude of saddle-node bifurcations. Near the transition to the desert state, many other unstable steady states influence the spatio-temporal behaviour of the vegetation field. It suggests that the self-organization mechanisms in such a model increases the complexity of the spatial and temporal correlations of the vegetation signal, which decreases the performance of the classical indicators. It is therefore interesting to investigate how network based indicators will perform in such a scale-dependent feedback model. Moreover, the network indicators will yield more information than looking alone at the patterns themselves as being possible indicators.

In the present study, the land–atmosphere model as presented in Konings et al. (2011) is used to test the performance of network based indicators regarding the desertification transition. This model couples land surface processes (Rietkerk et al., 2002) and the dynamics of the atmosphere boundary layer (Konings and Katul, 2010). It captures two important positive feedback mechanisms, the small-scale biomass-infiltration feedback (Rietkerk et al., 2002) and the large-scale precipitation-transpiration feedback (Entekhabi et al., 1992; Dekker et al., 2007). At small scales, increasing biomass is able to promote water infiltration rate, which provides more soil water and in turn maintains more biomass (Rietkerk et al., 2000). At large scales, increased precipitation leads to more biomass, which can increase transpiration rate and recharge water vapour in the atmosphere. Consequently more rainfall events can occur and increase the amount of precipitation (Entekhabi et al., 1992). In addition to these feedbacks, also the seasonal variability of rainfall, which is shown to be important in arid and semi-arid regions (Baudena and Provenzale, 2008; Good and Caylor, 2011; Siteur et al., 2014), is represented in the model.

Output from a large number of simulations with this model are used to reconstruct interaction networks from which early warning indicators of transitions are derived. The performance of these indicators is compared with those of classical indicators with the aim to understand the behaviour of these indicators near the desertification transition. In Section 2 the essential features of the land–atmosphere model and the complex network methodology are described. Results of the simulations of the land–atmosphere model are presented in Section 3.1 and the performance of the classical and network based early warning indicators is presented in Section 3.2. A summary and discussion of the results is given in Section 4.

2. Model and methodology

2.1. The land–atmosphere model

The land–atmosphere model (Konings et al., 2011) couples a one-column atmospheric boundary layer (ABL) model (Konings and Katul, 2010) with a scale dependent feedback vegetation model (Rietkerk et al., 2002). The ABL model is seasonally forced to capture the African monsoon variability (Konings et al., 2011). The vegetation model considers the interactions among surface water, biomass dynamics and soil moisture (Rietkerk et al., 2002). The surface energy balance contains the turbulent momentum and moisture exchange between the land and atmosphere (Konings et al., 2011). In this study, state-dependent stochastic noise is included for biomass, surface water and soil moisture to represent unresolved processes (Dakos et al., 2011; Tirabassi et al., 2014); the detailed equations of the model are presented in Appendix A. A full description of the model can be found in Konings et al. (2011).

The fundamental characteristic of the land–atmosphere coupling is the water and energy exchange between the land surface and the ABL. The vegetation model simulates the biomass dynamics and determines the sensible and latent heat fluxes. The sensible heat flux (H) changes the boundary layer height (h) while the latent heat flux (LE) affects the specific humidity (q) of the atmosphere. Convective rainfall occurs when h crosses the Level of Free Convection (LFC) and the Lifting Condensation Level (LCL). The LFC is the altitude where the lifted parcels become buoyant, while the LCL is the height where the condensation starts. When rainfall occurs, the amount of rainfall is determined by the total moisture content in the atmosphere and a rainfall efficiency (η, Eq. (A.7)). The parameter η will be the main control parameter in the model and controls (together with other processes as transpiration, etc.) the total amount of annual precipitation (Konings et al., 2011). When η =1, the simulated mean annual precipitation is approximately 365 mm yr^{-1}. Note that the mean annual precipitation (P) is dependent on the strength of the vegetation–precipitation feedback. Thus η is used as an index to represent the dryness of climate.

The model was applied on 75 × 75 grid cells. Surface runoff, soil water spread and biomass colonization were considered as main land surface processes (Eqs. (A.8), (A.9) and (A.15)). The energy balance was calculated for each grid cell. However, spatial averaged sensible and latent heat fluxes were used to estimate water and energy exchanges between the land and atmosphere. To extract biomass equilibria under specific climate, the simulation started with a relative high initial biomass. The time step for atmospheric convection was 150 s, while biomass was updated once per day. The model was run until the biomass state reached equilibrium. As a criterion for reaching the equilibrium, we required that the maximum (over the whole grid) relative difference of the annual mean values of the biomass field between two neighbouring years was less than 0.5%.

The land–atmosphere model accounts for the annual cycle of solar radiation. Moreover, the observed climate forcing data (slope γ and intercept ϕ of the free atmosphere for specific humidity q and potential temperature θ, see Appendix A) contains seasonal atmospheric variability. To remove strong seasonal correlations due to forcing in the biomass time series B_i^n, where i refers to a location in space (i.e., a specific grid cell) and n to the time index, the average over M years (M = 5 in this paper) is removed for each day of the year. More specifically, for daily data with $n(j, k) = 365 \times (j-1) + k$ (leap years ignored), the detrended time series B_i^n is determined from

$$B_i^{n(j,k)} = B_i^{n(j,k)} - \frac{1}{M}\sum_{j=1}^{M} B_i^{n(j,k)}. \quad (1)$$

The correlation coefficient between B_i^n and B_i^n is less than 0.2 in all randomly selected values of i, implying that the annual cycle is successfully removed from each time series. Note that the detrended biomass B_i^n can have negative values as it is an anomaly with respect to the seasonal cycle. All biomass time series referred to below in this paper are seasonally detrended.

2.2. Early warning indicators

'Critical slowing down' is demonstrated as the essential character of dynamic systems approaching a critical transition (Scheffer et al., 2009). This theory focuses on the recovery rate of a system when it turns back to the equilibrium state from a small perturbation. If the system state is far from the tipping point, the

attractor that drags the system back to its equilibrium state is strong and leads to a short recovery time. Once the system shifts to the bifurcation threshold, the recovery rate declines as the attractor becomes weak. One significant consequence is that both the variance and the lag-1 autocorrelation coefficient of the system time series increase dramatically when the system moves towards the tipping point.

Theoretical model studies reveal that both variance and lag-1 autocorrelation coefficient are ideal statistical indicators to grasp the 'critical slowing down' of a system before critical transition occurs (Dakos et al., 2008, 2011; Scheffer et al., 2009). More convincing evidences are from an aquatic food web experiment (Carpenter et al., 2011), where both variance and recovery rate of daily chlorophyll are found to increase significantly before the upcoming critical transition.

In this study, we only use the lag-1 autocorrelation coefficient to represent the 'critical slowing down' in the ecosystem. For a specific grid cell i ($i \in 75 \times 75$), we select the last 5-year time series of daily biomass after annual cycle detrending (see Section 2.1). The lag-m autocorrelation function $R_i(m)$ of grid cell i is given by

$$R_i(m) = \frac{\sum_{n=1}^{N-m}(B_i^n - \overline{B}_i)(B_i^{n+m} - \overline{B}_i)}{\sum_{n=1}^{N}(B_i^n - \overline{B}_i)^2}, \tag{2}$$

where $N = 365M$ is the total length of the time series and $\overline{B}_i$ is the mean of the time series. Critical slowdown is associated with an increase in the lag-1 autocorrelation $R_i(1)$.

Early warning signals also can be captured from the spatial correlations of system units (Scheffer et al., 2009; Dakos et al., 2010), which raise significantly when the state approaches to the tipping point (Dakos et al., 2011; Tirabassi et al., 2014). For a special group of dynamic systems (e.g., activator–inhibitor system (Turing, 1952; Rietkerk and van de Koppel, 2008) and cyclic dominated system (Szolnoki et al., 2014)) regular spatial patterns are formed under the impact of specific feedback mechanisms (Klausmeier, 1999; Caldarelli, 2007; Rietkerk et al., 2002; Kéfi et al., 2007a,b; Siteur et al., 2014b). Kéfi et al. (2007a) demonstrated that the distribution of vegetation patches obeyed the power law in the arid ecosystems of Mediterranean, which can extend to a vast group of dynamics systems governed by the Matthew effect (Clauset et al., 2009; Perc, 2014). The number and size of vegetation patches are proposed as ideal indicators for critical transitions, however this approach is not universally applicable to all dynamic systems (Pascual and Guichard, 2005; Dakos et al., 2010).

To determine changes in spatial correlation of the biomass often Moran's coefficient is used (Dakos et al., 2011). As shown in Appendix A, the total number of locations in the vegetation model $K = 75 \times 75$; Moran's coefficient at time n is then given by

$$I^n = \frac{K}{\sum_{ij} g_{ij}} \frac{\sum_{ij} g_{ij}(B_i^n - \overline{B}^n)(B_j^n - \overline{B}^n)}{\sum_i (B_i^n - \overline{B}^n)^2}, \tag{3}$$

where $g_{ij} = 1$ if node i and j ($i, j \in [1, 75 \times 75]$) are neighbours and $g_{ij} = 0$ otherwise. Furthermore, $\overline{B}^n$ is the spatial averaged biomass B at time index n. Here we only use the spatial distribution of the biomass at the last time step of the simulation (i.e., $n = N$).

The new element in this paper is to consider early warning indicators based on complex networks (Caldarelli, 2007), which are composed of nodes and links (or edges). In this study, the nodes are the $K = 75 \times 75$ grid cells of the vegetation model. To determine the links between two nodes i and j, we calculate the lag-0 Pearson cross correlation coefficients C_{ij} of the biomass time series at these nodes. Only the last 5-year daily biomass values are used for the calculation of C_{ij}. The nodes i and j are considered to be linked if the correlation $|C_{ij}|$ is higher than a certain threshold value $\tau > 0$. This threshold is determined by a significance analysis and for all the results below, $\tau = 0.7$ guarantees significant correlations with a p-value smaller than 0.05.

The network is next represented as a graph having $K = 75 \times 75$ nodes where the links are described by an adjacency matrix **A**. This is a $K \times K$ symmetric matrix where the element A_{ij} is given by

$$A_{ij} = \mathcal{H}(|C_{ij}| - \tau). \tag{4}$$

The quantity $\mathcal{H}$ is the Heaviside step function. Here $A_{ij} = 1$ (= 0) indicates that nodes i and j are linked (not linked). Fig. 1 provides an example of small network where the circles represent the (12) nodes and the red solid curves represent the links between the nodes.

By the network reconstruction, the analysis of spatio-temporal correlations in the biomass field is transformed into the analysis of topological properties of the graph (such as in Fig. 1) of the network. In this study, we focus on three topological properties: degree, assortativity and clustering.

The degree, denoted by d_i ($i \in [1,K]$), is the number of nodes that are linked with the specific node i, as:

$$d_i = \sum_{j=1}^{K} A_{ij}. \tag{5}$$

For instance, in Fig. 1 the degree of node i is 3. Note that the self correlation is ignored, thus the value of d_i varies from 0 to $K - 1$. The maximum value occurs when all nodes are significantly correlated.

The assortativity (a_i) is the average degree of the neighbours of node i and given by

$$a_i = \frac{1}{d_i} \sum_{j=1}^{K} A_{ij} d_j. \tag{6}$$

In Fig. 1, node i has three neighbours, the degree of each neighbour is 2 and hence the assortativity of node i is 2. The assortativity measures the second stage relations of the specific node in the network and values of a_i vary between 0 and $K - 1$.

The clustering coefficient (c_i) of node i is the ratio of the number of links among the neighbours of node i to the number of possible

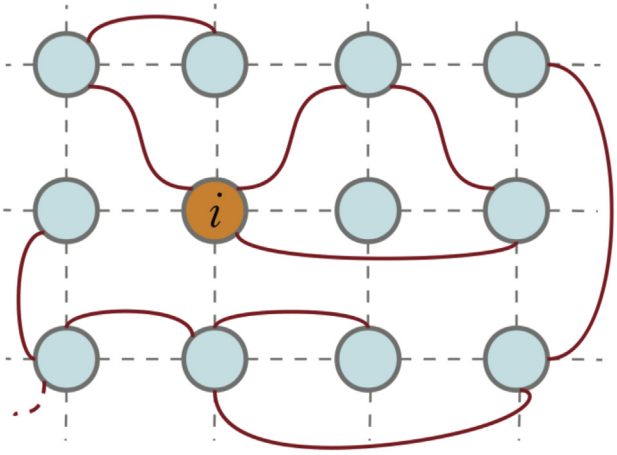

Fig. 1. Diagram to illustrate a complex network and its properties (from Tirabassi et al., 2014). Circles indicate the grid cells of B and form the nodes of the network. Solid lines indicate the links between the nodes. Node i has degree $d_i = 3$, clustering coefficient $c_i = 0.33$ and assortativity $a_i = 2$. (For interpretation of the references to colour in this sentence, the reader is referred to the web version of the article.)

links among its neighbours. The formula for c_i is:

$$c_i = \frac{1}{d_i(d_i-1)} \sum_{j=1}^{K} \sum_{l=1}^{K} A_{ij} A_{jl} A_{li}. \quad (7)$$

For example in Fig. 1, node i has three neighbours. Two of its neighbours are linked but there are three possible links among these neighbours. Thus the clustering coefficient is 1/3 =0.33. Values of c_i vary between 0 and 1 and the maximum value occurs when all neighbours of node i are linked.

3. Results

Before any early warning indicator can be applied, the different equilibrium states of the model and how simulated precipitation and biomass equilibrium fields change with the rainfall efficiency (η) have to be determined; this is presented in Section 3.1. Subsequently, the classical and network based indicators are applied to the simulated biomass time series in Section 3.2 and we next investigate their capabilities to serve as early warning signals of transitions between equilibria in the model (Section 3.3).

3.1. Equilibria in the land–atmosphere model

In the land–atmosphere model, the frequency and intensity of rainfall is determined by the water and energy transported from the land surface processes. As mentioned above, we use the rainfall efficiency η as the measure of the dryness of the climate (Konings et al., 2011). For values of η in the range from 0.7 to 1.0, branches of equilibrium solutions of the model were computed. By taking different initial conditions for similar values of η, different multiple equilibria were found. For instance, in the case of η = 0.84, a desert equilibrium is found from a high biomass initial condition. However, an equilibrium state with vegetation cover can be reached from the equilibrium state obtained with η = 0.85. As our main aim is to determine the performance of the early warning indicators near the desertification transition, it is not necessary to reveal all branches of equilibria in the model.

In Fig. 2, part of the bifurcation diagram of the model is plotted, showing the relation between rainfall efficiency η and the mean daily rainfall P and the equilibrium mean biomass B of the equilibria. The values of P and B are both spatially and temporally averaged using the data of the last five years of each model simulation. The dots in Fig. 2 indicate the actual values of η used and branches of equilibria are labelled L1–L7. Along each branch, B decreases with η and branches overlap for certain intervals of η. The desertification transition appears near η = 0.79, at the left end of branch L2, from where the equilibrium biomass shifts considerably from approximately 1 g m^{-2} to zero.

A different view on the properties of the solutions on the branches is obtained from Fig. 2B where P is plotted versus η. The positive vegetation–precipitation feedback leads to a high correlation between B and P. However, P does not drop to zero at branch L1 as soil evaporation exists and maintains a weak precipitation feedback. The correlation between P and B along the branches can also be clearly seen in the P–B diagram (Fig. 2C). By comparing this to the same diagram without land–atmosphere coupling (Dakos et al., 2011), we deduce that the 'gaps' in the P–B relation are caused by the vegetation–precipitation feedback. This suggests that abrupt shifts of the hydrological processes (i.e., precipitation and evapotranspiration) might be hidden in the smooth curve found between mean annual precipitation and maximum woody cover in Sankaran et al. (2005). Note that all abrupt transitions found in the model are subcritical (so-called catastrophic transitions or critical transitions), implying that such state transitions cannot be recovered simply by changing η back to the original value.

The only overlap of branches in Fig. 2C is that of the branches L5 and L7 where the different solutions are associated with slightly different rainfall rates (Fig. 2B). At the beginning of the simulation, biomass dynamics, transpiration amount and rainfall frequency are almost the same (see Fig. B.1 in Appendix B). However, more water vapour is stored in the atmosphere in the lower η case (branch L5) as less precipitation is generated but the water vapour recharge from transpiration is almost the same as the higher η case (branch L7). Such water vapour accumulation process lasts until an extra precipitation occurs (Fig. B.1B), which leads to a huge difference of the simulated B (Fig. B.1A). It means that with the similar P, a lower η in L5 has higher rainfall frequency and yields higher B than higher η in L7. The results agree with other findings about the effect of rainfall frequency on biomass dynamics (Baudena and Provenzale, 2008; Siteur et al., 2014). Moreover, the range of P ($0.6 < P < 1.0$ mm d^{-1}) where patterned biomass exists in Fig. 2C is narrower than in the vegetation model without land–atmosphere coupling ($0.3 < P < 1.3$ mm d^{-1}), which coincides with the findings from Dijkstra (2011).

Typical vegetation patterns on each branch are shown in Fig. 3 and most overlap between branches occurs (between L2 and L4) when vegetation patterns are spots. For η in the interval [0.85–0.9], the environment can sustain numerous equilibria with a wide

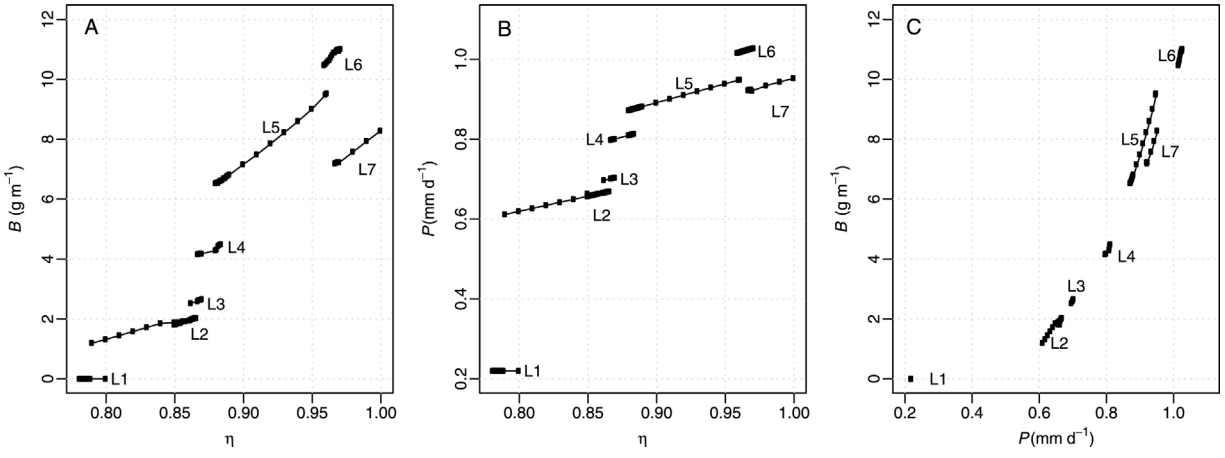

Fig. 2. The relation between the rainfall efficiency η, the mean biomass B (panel A) and the mean precipitation P (panel B), with a P–B diagram in panel C. Solid lines indicate equilibria of the model and the dots indicate the actual values found in the model simulations.

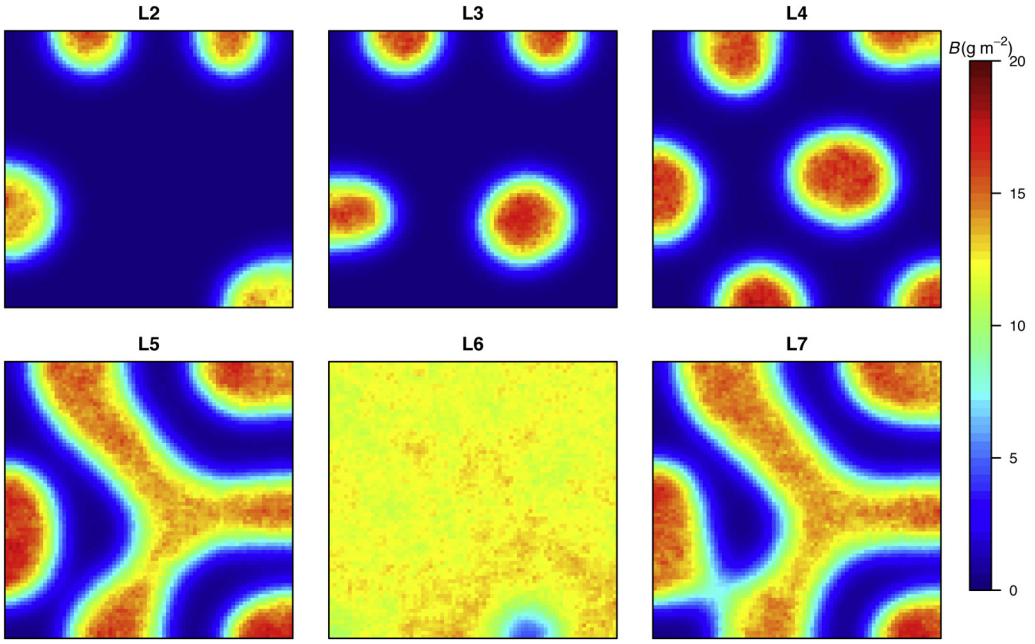

Fig. 3. Equilibrium biomass patterns at different branches shown in Fig. 2. The plots are based on the biomass at the last time step of the simulation. The specific rainfall efficiency values η are: L2:0.79; L3:0.857; L4:0.87; L5:0.92; L6:0.962; L7:0.98. (For interpretation of the references to colour in this figure legend, the reader is referred to the web version of the article.)

range in spot numbers. Along a branch the spot number remains constant but different branches are associated with different spot numbers. Qualitatively similar behaviour was found by (Dijkstra, 2011) in another coupled land–atmosphere model (Dekker et al., 2007). Siteur et al. (2014b) revealed that vegetation can adjust to the environment by changing biomass of patches or by shifting wavelength. The change of wavelength is associated with a jump between the branches. Only spots at the border of the domain survive along branch L2, which is different to the spot patterns on other branches. This is consistent with the results in Dijkstra (2011), where also patterns with only border spots can be sustained under low rainfall.

3.2. Early warning indicators

Fig. 4 shows the two classical indicators, the lag-1 autocorrelation and Moran's coefficient versus P (using the values in Fig. 2B) and the behaviour of the two indicators is similar. A sharp increase with decreasing η occurs along branch L6, implying that the indicators are sensitive to the shift of biomass from a homogeneous distribution to a labyrinth patterns (Figs. 2 and 3). The indicators drop sharply from L6 to L5 and then gradually increase until L2. When the state is approaching the desertification transition along L2, the value of indicators drops considerably. The trend coincides with the results from Dakos et al. (2011) where both the classical indicators do not smoothly increase with the decrease in rainfall and a sharp drop occur before the upcoming desertification. Even though the sharp decrease of the indicators is a clear early warning signal of the upcoming critical transition, their behaviour is quite irregular and can easily lead to a false alarm.

We now turn to the network based indicators and show in Fig. 5A the distribution of the degree of a network determined for a value of η along the different branches (Fig. 3). Two values of η (0.79 and 0.85) are chosen along the branch L2 to illustrate the large change in the degree distribution before the desertification transition. All distributions are bimodal with the first peak fixed at zero while the second peak increases from approximately 500 (L6)

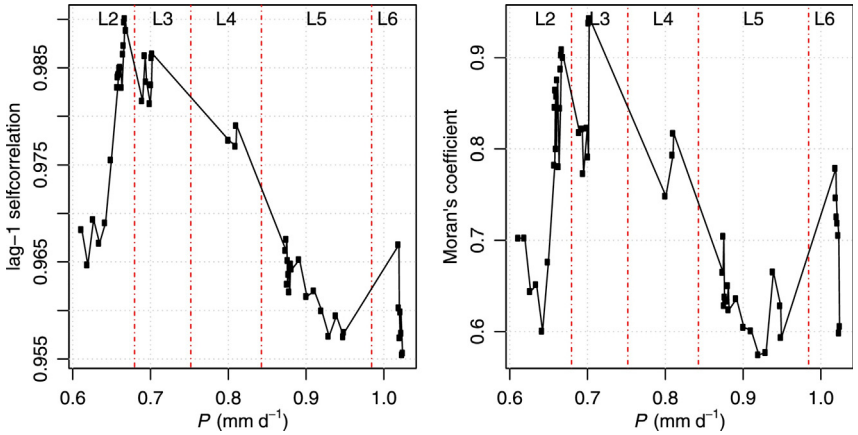

Fig. 4. The behaviour of the classical indicators versus P with in the left panel the lag-1 autocorrelation (Eq. (2)) and in the right panel Moran's coefficient (Eq. (3)). Moran's coefficient is based on the spatial distribution of biomass at the last time step of the simulation. Red dashed lines reveal the regions of different branches shown in Fig. 2. (For interpretation of the references to colour in this figure legend, the reader is referred to the web version of the article.)

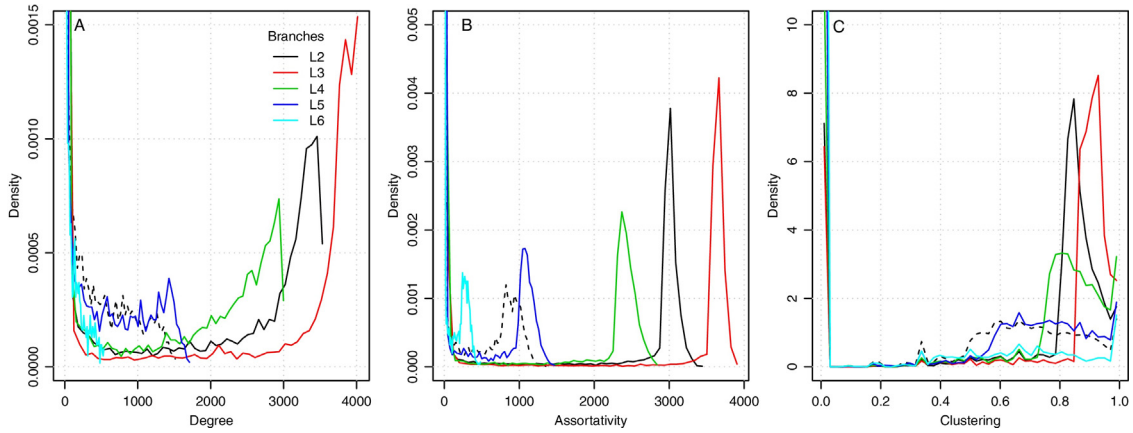

Fig. 5. The distribution of the network properties (A) degree, (B) assortativity and (C) clustering coefficient along the different branches (distinguished by the colours). The solid and dashed curves represent the two samples from L2. The specific η of the samples are: L2:0.79 (dashed) and 0.85 (solid); L3:0.869; L4:0.87; L5:0.883; L6:0.968. (For interpretation of the references to colour in this figure legend, the reader is referred to the web version of the article.)

to 4000 (L3) and then decreases along the branch L2. Similar behaviour occurs for the assortativity of the networks (Fig. 5B) and the clustering coefficient (Fig. 5C). As in Tirabassi et al. (2014), the network based indicators will be determined from the properties of the distribution of each network quantity.

Fig. 6 shows these network based indicators as a function of *P*. Degree, assortativity and clustering are listed in columns. The properties of the distributions (mean, standard deviation, skewness and kurtosis) are plotted in rows. All moments are determined by the shift of the bimodal distribution (Fig. 5A). Both the mean and variance of the degree distribution how a similar variation with *P* as the classical indicators (Fig. 2). However, the relative drop of the network based indicators near the desertification transition (e.g., from 2000 to 200 for the mean degree) is much larger than that for the classical indicators. The skewness (Fig. 6) is influenced by the areas of the two peaks in the degree distribution (Fig. 5A). With decreasing *P*, the skewness degree drops until −1 and sharply increases before the desertification transition. Although the skewness degree varies over a small range, the sign change can be a useful early warning indication for the desertification transition. Note that such sign change only occurs along branch L2. The kurtosis of the degree distribution also presents a useful indicator as it is

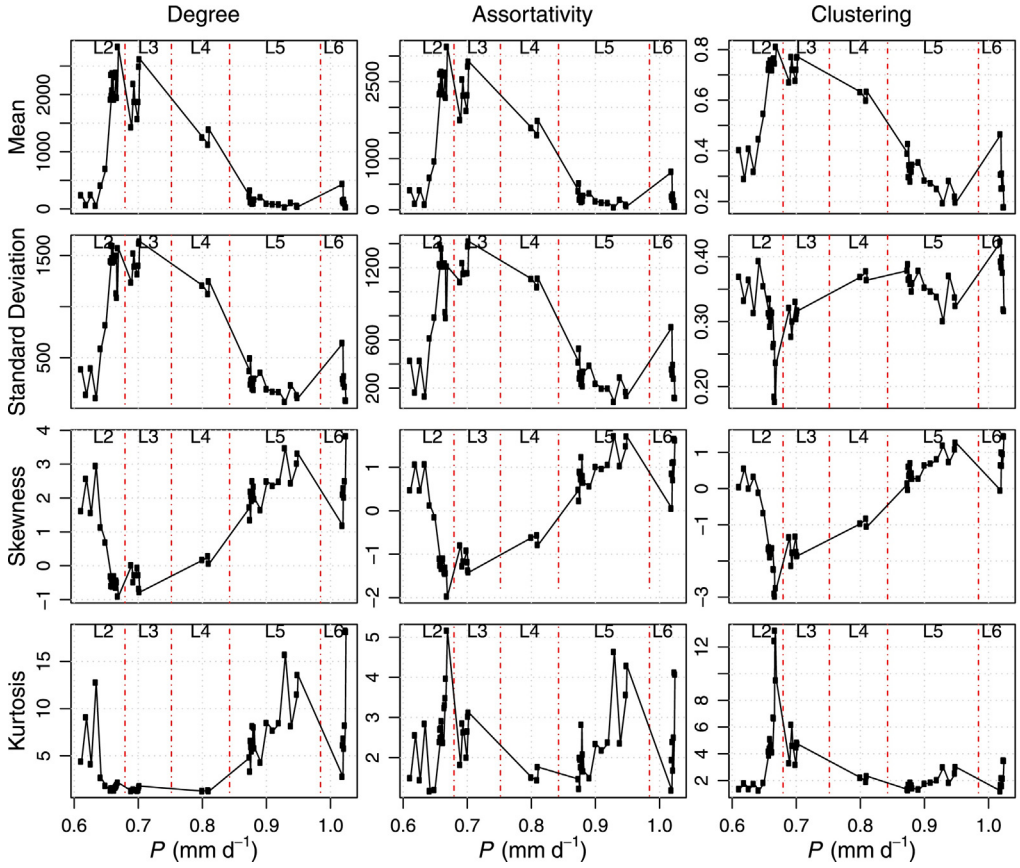

Fig. 6. Network based indicators as a function of mean annual rainfall *P*. Three network variables are listed in columns and different statistic indicators are listed in rows. The diagrams are divided by red dashed lines into six regions for different branches. (For interpretation of the references to colour in this figure legend, the reader is referred to the web version of the article.)

small and near constant at high P end of branch L2 and then increases sharply with decreasing P.

In the middle column of Fig. 6 the properties of the distribution the network assortativity is shown. Bimodality is also found in the assortativity (Fig. 5B) where the movement of the second peak is the same as that of the degree distribution. The behaviour of the mean, standard deviation and skewness of the assortativity distribution are similar to that of the degree. The kurtosis behaves different in that it decreases with decreasing P and is not constant at the high P end of branch L2. It is interesting that the behaviour of the skewness of the assortativity is similar to that found in the local positive feedback model (Tirabassi et al., 2014). This suggests that this indicator might be a more broadly applicable signal for transitions in a wide range of ecological models.

Finally, in the right column of Fig. 6, the properties of the distributions of clustering coefficient of the networks are shown. The behaviour of the mean, skewness and kurtosis of the clustering coefficient is very similar to that of the assortativity; the standard deviation, however, increases with decreasing P. The position of the second peak in the clustering distribution moves only slightly with P (Fig. 5C), which leads to relatively small changes in mean and standard deviation (Fig. 6). However, the kurtosis of the distribution changes dramatically and leads to a sharp peak when the state shifts from L3 to L2 (Fig. 6).

3.3. Quality measures of the indicators

At first sight, both classical and network indicators could be used as early warning indicators of the desertification transition. However, the sensitivities of these indicators to changes in P are quite different. It is hard to distinguish whether sudden changes in an indicators contains a 'real' early warning signal or is just due to the strong variation of this quantity. Hence it is important to determine and evaluate measures of quality of the indicators. We propose two measures to assess the quality of the indicators. Each of them can be written in the form

$$D = \frac{|\Psi_1 - \Psi_2|}{\Psi_1 + \Psi_2}, \tag{8}$$

where Ψ_1 and Ψ_2 are the two specific quantities that are compared. A high (low) value of D implies a large (small) difference between Ψ_1 and Ψ_2 and vice versa.

The first measure, denoted by D_m, focuses on the sudden change of an indicators along the L2 branch (cf. Fig. 4). It evaluates the magnitude of the difference between the mean of the specific indicator before and after the sudden shift in L2. Points with $\eta \leq 0.82$ are classified as the states after the sudden shift while points with $\eta \geq 0.851$ are classified as the states before the sudden shift. For each indicator, the mean values of the two point groups are set as Ψ_1 and Ψ_2 in Eq. (8) to calculate D_m. Indicators with a large shift along L2 will have higher values of D_m. Note that the mean value of the skewness may be negative, which is not accounted in this assessment.

The second measure (D_v) considers the difference of variances before and after the sudden shift in L2. The two point groups are classified as for the D_m measure. Low values of D_v indicate that the specific indicator has a significant variation along the branch L2 and hence is less suited as an early warning signal.

Table 1 presents the assessment of all indicators by the two measures: a good indicator ideally has high values of both D_m and D_v. The classical indicators have typically much lower values of D_m than the network indicators. It implies that the abrupt drops of network indicators are more significant than that of classical ones. Highest values of D_m are found for the mean degree and the mean assortativity distribution. Note that although D_m of the skewness is not available, the sign change is already a significant early alarm for upcoming desertification. Higher values of network indicators in the D_v measurements indicate that they have stronger capability to distinguish the abrupt shift from the local variation. Indicators with high D_v are the kurtosis of the degree and of the clustering. The mean and skewness of the degree also show remarkable D_v. In general, early warning signals of network indicators have a higher quality than the classical indicators.

4. Summary and discussion

Abrupt regime shifts are found widely in real ecosystems (Scheffer et al., 2001; Ripple and Beschta, 2006; Rietkerk et al., 2004; Kefi et al., 2008; Móréh et al., 2009; Higgins and Scheiter, 2012). These transitions are caused by different biophysical or biochemical feedback mechanisms (Cochrane et al., 1999; Bonan, 2008; Zeng and Yoon, 2009; Dekker et al., 2010; Dekker, 2013; Perc, 2014), while the impacts on the local climate are profound and may lead to unexpected catastrophe. Moreover, observations provide direct or indirect evidence that multi-equilibria of ecosystem states exist under similar climate regimes (Scheffer et al., 1993, 2012, 2014; Hirota et al., 2011; Staver et al., 2011b; Yin et al., 2014), which reveal the potential occurrence of critical transitions in current ecosystems. To predict upcoming tipping points is of large interest, and therefore early warning indicators should be developed and analysed for different systems.

The 'critical slowing down' is demonstrated as the essential phenomena when a system is approaching the tipping point (van Nes and Scheffer, 2007; Dakos et al., 2008; Scheffer et al., 2009). Consequently, numerous statistical indicators based on this theory are proposed and successfully yield early warning signals for critical transitions in ecological bifurcation models (Dakos et al., 2011). But there are still two crucial questions unclear. Firstly, although these so-called classical indicators successfully predict whether the system is shifting towards a tipping point, the gradual increase of classical indicators cannot provide explicit information about how far the current state is from the tipping point. Thus we need other indicators that can release strong signals just ahead of the critical transition (Tirabassi et al., 2014). Secondly, these tested classical ecological models only represent a few biophysical or biochemical feedbacks. It is interesting and important to investigate models with multi feedback mechanisms at different spatial and temporal scales.

In this study, we evaluated the performance of early warning indicators for the desertification transition in a coupled land–atmosphere model. In contrast to other ecological models (Dakos

Table 1
Evaluation of the quality of the early warning indicators by the two different measures D_m and D_v.

Variable	Indicators	Type	D_m	D_v
Degree	Mean	Network	0.871	0.758
	SD	Network	0.696	0.046
	Skewness	Network	–	0.884
	Kurtosis	Network	0.653	0.992
Assortativity	Mean	Network	0.821	0.558
	SD	Network	0.609	0.124
	Skewness	Network	–	0.345
	Kurtosis	Network	0.197	0.120
Clustering	Mean	Network	0.357	0.697
	SD	Network	0.112	0.592
	Skewness	Network	–	0.591
	Kurtosis	Network	0.619	0.991
	Lag-1 autocorrelation	Classic	0.010	0.216
	Moran's coefficient	Classic	0.117	0.345

et al., 2011; Tirabassi et al., 2014), multiple overlapping branches of equilibria were found in this model. Two criteria were applied to assess the quality of early warning indicators and the results showed that the network based indicators had a relatively high quality compared to the classical ones.

The land–atmosphere coupled model (Konings et al., 2011) captures two feedback mechanisms. The local infiltration positive feedback results in regular vegetation patterns (Rietkerk et al., 2004), which changes with the total amount of precipitation. The vegetation–precipitation feedback leads to the discrete *P*–*B* lines in Fig. 2C. Multiple stable branches (L2, L3 and L4) are found after vegetation patterns shift from labyrinth to patches and transitions are caused by the change of number or position of patches (Dijkstra, 2011; Siteur et al., 2014b). The catastrophic shift to desertification (from L2 to L1 in Fig. 2) is associated with the disappearance of the boundary patches.

This behaviour of the model equilibria explains why most of indicators increase from L5 to L4, then keep a near constant value down to L2 and drop sharply before the desertification (Dakos et al., 2011). The indicators do detect potential critical transitions as they change substantially when multiple stable states exist (from L5 to L2). As was found in Dijkstra (2011), all branches of equilibria already exist with the infiltration feedback. The vegetation–precipitation feedback only shifts the branches and hence does not appear to be important for the existence of the desertification transition, but determines the value of *P* for which this occurs.

The behaviour of the classical indicators is similar to that of most network based indicators. However the network based indicators are more sensitive to upcoming critical transitions and the signals can be easier distinguished from local variations. This does not mean that classical indicators can be abandoned as they provide early warning signals at an very early stage of transition (Scheffer et al., 2009; Dakos et al., 2011). However, the network based indicators provide more peaky signals when the critical transition is approached (Tirabassi et al., 2014) and hence form a useful addition to the classical indicators.

However it is still unclear if warning signals only associate with multiple stable states. Kéfi et al. (2013) found that classic indicators also yielded early warning signals for supercritical transitions, which is non-catastrophic as abrupt shifts are reversible. As non-catastrophic transitions are not found in this study, we cannot confirm whether network indicators can provide distinct performances to them. In further studies, however, it is very interesting to examine the network approach in classic models that contain non-catastrophic transitions (Dakos et al., 2011; Kéfi et al., 2013).

More importantly, theoretical studies are able to show light on crucial scientific questions. Although vast fruitful results are revealed from ecological models (van Nes and Scheffer, 2007; Scheffer et al., 2009; Dakos et al., 2011; Tirabassi et al., 2014), how to apply these knowledge on real world systems is still a challenge. Firstly, field experiments are difficult to implement. Carpenter et al. (2011) tested classical indicators in a food web experiment, in which top predators are added artificially to cause a regime shift in a human manipulated aquatic ecosystem. The success of the experiment requires a reference ecosystem (similar in climate, food web, etc.) to split potential effects from external drivers. Long-term measurements with high frequency are also needed to calculate these indicators. Moreover, the elegance of this experiment is that the interactions among elements in the food web is relatively simple and clear. If we extend this experience to an experiment with different spatial and temporal scales, the complexity in interactions and feedbacks will increase dramatically.

Secondly, critical transitions are widely predicted but direct observations are lacking. Large scale observations via satellite only last for several decades, which is very short compared to the time scale of occurred critical transitions (Kröpelin et al., 2008). Nevertheless, ecologists established models to explain these observed vegetation patterns and warned for possible critical transitions (Rietkerk et al., 2004; Kéfi et al., 2007b; Staver et al., 2011a; Hirota et al., 2011). Thus, in a next step, it is vital to use both classical and network approaches to estimate how far the current ecosystem is from its tipping point.

Acknowledgements

We wish to thank two anonymous reviewers for their helpful comments. We also like to thank Utrecht University for financial support of this research through a Focus and Mass project within the Sustainability theme. H.D. acknowledges the support of the LINC project (no. 289447) funded by EC's Marie-Curie ITN program (FP7-PEOPLE-2011-ITN). The authors thank Giulio Tirabassi for providing the software to reconstruct and analyse the networks.

Appendix A. Model description

A.1. Atmospheric boundary layer model

The potential temperature (θ) and the specific humidity (q) varies with the height of the atmospheric boundary layer (ABL). For simplicity the model assumes that the energy and water vapour are well mixed in the ABL. Consequently θ and q are constant in the ABL. On the top of ABL, both θ and q are assumed to have a linear relation with the height above the surface z, as:

$$\theta(z) = \gamma_\theta z + \phi_\theta \tag{A.1}$$

$$q(z) = \gamma_q z + \phi_q, \tag{A.2}$$

where γ and ϕ are slope and intercept, respectively.

The change of the height of the ABL (h) in time t is as a function of latent heat flux,

$$\frac{\mathrm{d}h}{\mathrm{d}t} = \frac{(1+2A)\overline{(\theta'\omega')_s}}{\gamma_\theta h}, \tag{A.3}$$

where $\overline{(\theta'\omega')_s}$ is the sensible heat flux from the surface; A is the ratio of the sensible heat flux at the top of the ABL to the surface sensible heat flux, which is called Tennekes parameter and assumed as constant (0.2).

When the ABL grows, the heat and humidity fluxes in the top of the ABL is proportional to the difference between the value on the top of the ABL and the value below the fluxes. The temperature and humidity of the ABL can be estimated by the conservation equations:

$$h\frac{\mathrm{d}\theta}{\mathrm{d}t} = \overline{(\theta'\omega')_s} + (\gamma_\theta h + \phi_\theta - \theta)\frac{\mathrm{d}h}{\mathrm{d}t}, \tag{A.4}$$

$$h\frac{\mathrm{d}q}{\mathrm{d}t} = \overline{(q'\omega')_s} + (\gamma_q h + \phi_q - q)\frac{\mathrm{d}h}{\mathrm{d}t}, \tag{A.5}$$

where $\overline{(q'\omega')_s}$ is the sensible heat flux at the surface. The $\overline{(\theta'\omega')_s}$ and $\overline{(q'\omega')_s}$, which are calculated in the vegetation model, are described in Appendix A.2.

The precipitation occurs only when h crosses the height of the Level of Free Convection (LFC) and Lifting Condensation Level (LCL). Another condition, $z/L \geq 5$, is included in the model of Konings et al. (2011) to make sure that the air parcels are able to rise from the LFC to the LCL. Here L is the Obukhov length:

$$L = \frac{u_*^3\theta}{\kappa_v g\overline{(\theta'\omega')_s}}, \tag{A.6}$$

where $z = h/2$ is the centre of the ABL; κ_v is von Karman's constant; g is the acceleration due to gravity; u_* is the friction velocity.

The amount of rainfall is proportional to the total water vapour in the atmosphere column. The moisture over the height of the free atmosphere is also taken into account. Following Konings et al. (2011) to prevent the uncertainties from the free atmosphere, the model accounts for the water vapour in the atmosphere column with double height of the ABL, as:

$$P = \eta_{\text{steady}}\eta\int_0^{2h} q\,\mathrm{d}z, \tag{A.7}$$

where P is the amount of rainfall and the duration is set at 2 h; $\eta \in [0,1]$, called rainfall efficiency, is a free parameter to account for all factors that influences the rainfall process; η_{steady} (0.33) is a constant to fix the simulated mean annual precipitation at approximately 365 mm yr^{-1} when $\eta = 1$ (Konings et al., 2011).

A.2. Vegetation dynamics model

The vegetation model (Rietkerk et al., 2002) integrates the surface energy balance in the vegetation dynamics to simulate the water and heat feedback to the atmosphere (Konings et al., 2011). In this study, we consider a lattice with 75×75 grid cells. The dynamics of surface water content (O), soil water content (W) and biomass (B) are simulated in each cell with stochastic process (Dakos et al., 2011). The horizontal exchange of water and biomass are estimated at the boundary of neighbouring cells. The vertical fluxes of water and energy from the land to the atmosphere (e.g., transpiration, sensible heat flux, etc.) are averaged values of all grid cells.

Precipitation (P) is the only source that can recharge the water in the vegetation model. The O obtains water from P and re-distribute it spatially or vertically. The dynamical equation of O is written as:

$$\frac{\partial O}{\partial t} = P - \alpha_0 \frac{B + k_2 W_0}{B + k_2} O + D_O \nabla O + \sigma_O O \xi^O(t). \tag{A.8}$$

O can lose water due to infiltration (the second term in Eq. (A.8)). The infiltration rate is determined by current O and B (Rietkerk et al., 2002). α_0 is the maximum infiltration rate; k_2 is the saturation constant of infiltration; W_0 is the relative infiltration fraction of bare soil. $D_O \nabla O$ is the diffusion of the surface water O with diffusivity D_O. $\sigma_O O \xi^O(t)$ is the noise of O. The noise is a proportional to O. $\xi^O(t)$ is Guassian white noise with standard deviation $\sigma_O = 0.01$.

The soil water content W is recharged by infiltration of O and lost by evapotranspiration and deep soil drainage. The governing equation is:

$$\frac{\partial W}{\partial t} = \alpha_0 \frac{B + k_2 W_0}{B + k_2} O - E_t - E_s - r_w W + D_W \nabla W + \sigma_W W \xi^W(t). \tag{A.9}$$

The first term is the infiltration rate of O, which is the same as Eq. (A.8). E_t and E_s are vegetation transpiration and bare soil evaporation, respectively. $r_w W$ is the deep soil drainage, which is proportional to W with a constant rate r_w. The diffusion and noise term are similar to Eq. (A.8).

The E_t and E_s are linearly related with latent heat fluxes of vegetation and bare soil, respectively, as:

$$E_s = \frac{LE_s}{\lambda \rho_{\text{H}_2\text{O}}}, \tag{A.10}$$

$$E_t = \frac{LE_t}{\lambda \rho_{\text{H}_2\text{O}}}, \tag{A.11}$$

where $\rho_{\text{H}_2\text{O}}$ is the water density; LE_t and LE_s are latent heat fluxes of vegetation and bare soil, respectively, which are estimated by the Penman–Monteith equation, as:

$$LE = \frac{\Delta(R_n - G) + \frac{\rho c_p \text{VPD}}{r_a}}{\Delta + \gamma\left(1 + \frac{r_s}{r_a}\right)}. \tag{A.12}$$

LE is the latent heat flux of the bare soil or vegetation, which is determined by the parameterization of the surface resistance r_s. R_n is the net radiation; G is the soil heat flux; ρ is the air density; c_p is the specific heat capacity of the air; VPD is the vapour pressure deficit; Δ is the slope of the saturated vapour pressure to temperature; γ is the psychrometric constant, which is a function of the surface pressure and the latent heat of evaporation λ, as $\gamma = c_p P_s/(0.622\lambda)$. r_a is the aerodynamic resistance; r_s is the surface resistance. When calculating vegetation latent heat flux LE_t, the model use the stomatal resistance $r_s^{E_t}$ as r_s. When r_s represents the bare soil resistance $r_s^{E_s}$, the latent heat flux of the soil LE_s will be calculated.

The stomatal resistance $r_s^{E_t}$ is a function of W, VPD and leaf area index (LAI). The LAI is positive related with the biomass B. For simplicity Konings et al. (2011) assume a linear function as LAI = $\alpha_1 B$, which holds due to the low values in B in this semi-arid region. α_1 represents the constant ratio of LAI to B. The formula of $r_s^{E_t}$ is:

$$\frac{1}{r_s^{E_t}} = \frac{1}{r_{\min}^{E_t}} \frac{W}{W + k_1}(1 - m\log(\text{VPD}))\alpha_1 B, \tag{A.13}$$

where $r_{\min}^{E_t}$ is the minimum stomatal resistance per unit LAI; k_1 is the saturated water stress; m is a factor used to represent the increase rate of resistance with decreased VPD.

The soil resistance $r_s^{E_s}$ is calculated as:

$$\frac{1}{r_s^{E_s}} = \frac{1}{r_{\min}^{E_s}} \frac{W}{W + k_1}\left(1 - \frac{B}{B + k_3}\right), \tag{A.14}$$

where $r_s^{E_s}$ is the minimum soil resistance; k_3 is the constant used in the function to estimate the effect of biomass shade to soil evaporation.

The dynamics of biomass is determined by carbon assimilation rate and respiration. Carbon assimilation positively relates to the amount of biomass B and CO_2 gradient between inside and outside of the stomata, while the respiration rate is determined by B and the air temperature T_a. The formula is given as:

$$\frac{\partial B}{\partial t} = (g_{\text{CO}_2} c C_1 \alpha_1 B - Re(T_a)B)\frac{1}{\tau(W)} + D_B \nabla B + \sigma_B B \xi^B(t), \tag{A.15}$$

where g_{CO_2} is the stomatal conductance of CO_2; c is the CO_2 gradient between the atmosphere and the internal space of stomata; C_1 is the conversion rate between carbon gain and biomass growth. $Re(T_a)$ is the respiration rate with specific air temperature T_a. $\tau(W)$ indicates the drought adaption of the vegetation. The diffusion and noise term are similar to Eq. (A.8).

The stomatal conductance g_{CO_2} is determined by the opening of the stomata, which has a linear positive relation with E_t, as:

$$g_{\text{CO}_2} = \nu \frac{E_t}{q - q^*}, \tag{A.16}$$

where ν is the ratio of CO_2 stomatal conductance to H_2O stomatal conductance; q is the surface specific humidity; q^* is the saturated specific humidity. The respiration rate is governed by a Q_{10} function as:

$$Re(T_a) = R_b Q_{10}^{((T_a - 10)/10)}, \tag{A.17}$$

where R_b is the referred respiration rate at 10 °C. The $\tau(W)$ is given as:

$$\tau(W) = \frac{1}{4}\frac{W^2 + fk_4}{W^2 + k_4}, \tag{A.18}$$

where k_4 is a constant related to soil water; f is the metabolic rate without water. Note that the time step of the biomass dynamics is 1 day, which is different with the time interval (2.5 min) of the ABL and water simulations.

The surface energy budget is composed by net radiation R_n, sensible heat flux H, latent heat flux LE and soil heat flux G. The net radiation is calculated by:

$$R_n = (1-\alpha)R_s + \epsilon_s\sigma(\epsilon_a T_a^4 - T_s^4), \tag{A.19}$$

where α is the surface albedo, which is linearly interpolated between $\alpha = 0.25$ when $B = 0\ \mathrm{g\,m^{-1}}$ and $\alpha = 0.15$ when $B = 25\ \mathrm{g\,m^{-1}}$. σ is the Stefan–Boltzmann constant; ϵ_s and ϵ_a are emissivity of the surface and atmosphere, respectively. R_s is the incoming shortwave radiation. It is a function of number of day DOY, hour angle h_a and the latitude ϕ. It is given by:

$$R_s = \frac{R_0}{r^2}\cos\beta, \tag{A.20}$$

where R_0 is the solar constant; r is a factor to correct the distance between the earth and the sun; β is the solar zenith angle. The r is determined by the DOY as:

$$r = 1.0 + 0.017\cos\frac{2\pi}{365}(186 - \mathrm{DOY}). \tag{A.21}$$

The β is affected by the hour angle and the latitude ϕ, as:

$$\cos\beta = \cos\phi\cos h_a\cos\delta + \sin\phi\sin\delta, \tag{A.22}$$

where δ is the solar declension.

The sensible heat flux H is a function of surface resistance and the temperature gradient between the surface and the atmosphere:

$$H = \frac{\rho c_p}{r_a}(T_a - T_s), \tag{A.23}$$

where $r_a = h_{ra}/(z_o\kappa_v u_*)$. h_{ra} and z_o are the height of the surface layer and the surface roughness, respectively. The z_o is determined by the canopy height h_c as $z_o = 0.1h_c$ and $h_c = 0.05/(3B)$.

Table A.1
Values of parameters in the coupled land–atmosphere model.

Parameter	Value	Unit	Parameter	Value	Unit
A	0.2	–	κ_v	0.41	–
g	9.81	$\mathrm{m\,s^{-2}}$	η_{steady}	0.33	–
α_0	0.2	$\mathrm{d^{-1}}$	k_2	5	$\mathrm{g\,m^{-2}}$
W_0	0.2	–	D_O	100	$\mathrm{m^2\,d^{-1}}$
D_W	0.1	$\mathrm{m^2\,d^{-1}}$	D_B	0.1	$\mathrm{m^2\,d^{-1}}$
σ_O	0.01	–	σ_W	0.01	–
σ_B	0.01	–	r_w	0.08	$\mathrm{d^{-1}}$
$r_{\min}^{E_t}$	100	$\mathrm{s\,m^{-1}}$	$\rho_{\mathrm{H_2O}}$	1000	$\mathrm{kg\,m^{-3}}$
α_1	0.01	$\mathrm{g^{-1}\,m^{-2}}$	c	152	ppm
C_1	0.0017	$\mathrm{g\,mol^{-1}}$	R_b	0.1	$\mathrm{d^{-1}}$
Q_{10}	1.6	–	k_1	3.3	mm
m	0.6	–	k_3	2.5	$\mathrm{g\,m^{-2}}$
ν	0.0259	$\mathrm{mm\,m^{-2}\,mol^{-1}}$	f	0.04	–
k_4	10	mm	σ	5.6703×10^{-8}	$\mathrm{J\,s\,m^{-2}\,K^{-4}}$
ϵ_s	0.97	–	R_0	1353	$\mathrm{W\,m^{-2}}$
h_{ra}	25	m			

The land surface energy balance equation is:

$$R_n - \lambda\rho E_t - \lambda\rho E_s - G - H = 0, \tag{A.24}$$

where $G = 0.15R_n$ is the soil heat flux. There are three unknowns (R_n, H and T_s) in Eqs. (A.19), (A.23) and (A.24), from where the energy balance of the surface can be estimated. The simulated H and LE are used to determine the surface sensible and latent heat fluxes in the atmosphere model as:

$$\overline{(\theta'\omega')}_s = \frac{H}{\rho c_p}, \tag{A.25}$$

$$\overline{(q'\omega')}_s = \frac{LE}{\rho c_p}. \tag{A.26}$$

All parameters are listed in Table A.1.

Appendix B. Figure

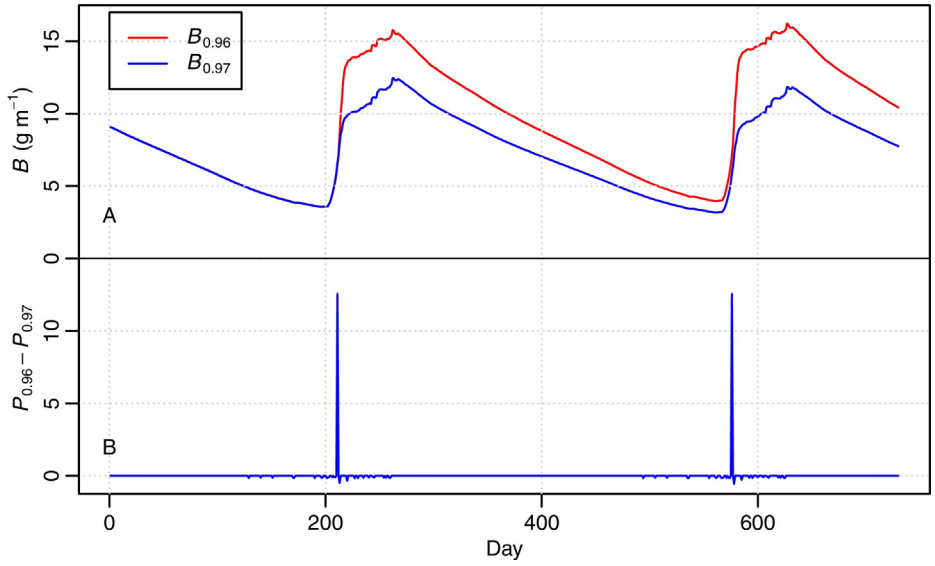

Fig. B.1. (A) Time series of daily spatial averaged biomass in the first 2-year simulation. Red and blue lines represent η =0.96 and 0.97, respectively. (B) Difference of daily rainfall between η = 0.96 and 0.97. The mean annual precipitation of η =0.96 and 0.97 is 346 mm and 338 mm, respectively. (For interpretation of the references to colour in this figure legend, the reader is referred to the web version of the article.)

References

Baudena, M., Provenzale, A., 2008. Rainfall intermittency and vegetation feedbacks in drylands. Hydrol. Earth Syst. Sci. 12, 679–689.

Bonan, G., 2008. Forests and climate change: forcings, feedbacks, and the climate benefits of forests. Science 320, 1444–1449.

Caldarelli, G., 2007. Scale-Free Networks: Complex Webs in Nature and Technology. Oxford University Press.

Carpenter, S.R., Cole, J.J., Pace, M.L., Batt, R., Brock, W.A., Cline, T., Coloso, J., Hodgson, J.R., Kitchell, J.F., Seekell, D.A., Smith, L., Weidel, B., 2011. Early warnings of regime shifts: a whole-ecosystem experiment. Science 332, 1079–1082.

Clauset, A., Shalizi, C., Newman, M., 2009. Power-law distributions in empirical data. SIAM Rev. 51, 661–703.

Claussen, M., Bathiany, S., Brovkin, V., Kleinen, T., 2013. Simulated climate–vegetation interaction in semi-arid regions affected by plant diversity. Nat. Geosci. 6, 954–958.

Cochrane, M.A., Alencar, A., Schulze, M.D., Souza, C.M., Nepstad, D.C., Lefebvre, P., Davidson, E.A., 1999. Positive feedbacks in the fire dynamic of closed canopy tropical forests. Science 284, 1832–1835.

Dakos, V., Kéfi, S., Rietkerk, M., van Nes, E.H., Scheffer, M., 2011. Slowing down in spatially patterned ecosystems at the brink of collapse. Am. Nat. 177, E153–E166.

Dakos, V., van Nes, E., Donangelo, R., Fort, H., Scheffer, M., 2010. Spatial correlation as leading indicator of catastrophic shifts. Theor. Ecol. 3, 163–174.

Dakos, V., Scheffer, M., van Nes, E.H., Brovkin, V., Petoukhov, V., Held, H., 2008. Slowing down as an early warning signal for abrupt climate change. Proc. Natl. Acad. Sci. U. S. A. 105, 14308–14312.

Dekker, S., De Boer, H., Brovkin, V., Fraedrich, K., Wassen, M., Rietkerk, M., 2010. Biogeophysical feedbacks trigger shifts in the modelled vegetation-atmosphere system at multiple scales. Biogeosciences 7, 1237–1245.

Dekker, S., Rietkerk, M., Bierkens, M., 2007. Coupling microscale vegetation-soil water and macroscale vegetation–precipitation feedbacks in semiarid ecosystems. Global Change Biol. 13, 671–678.

Dekker, S.C., 2013. Palaeoclimate: biodiversity-dominated feedback. Nat. Geosci. 6, 903–904.

Dijkstra, H., 2011. Vegetation pattern formation in a semi-arid climate. Int. J. Bifurc. Chaos 21, 3497–3509.

Entekhabi, D., Rodriguez-Iturbe, I., Bras, R., 1992. Variability in large-scale water balance with land surface–atmosphere interaction. J. Clim. 5, 798–813.

Good, S.P., Caylor, K.K., 2011. Climatological determinants of woody cover in Africa. Proc. Natl. Acad. Sci. U. S. A. 108, 4902–4907.

Higgins, S.I., Scheiter, S., 2012. Atmospheric CO_2 forces abrupt vegetation shifts locally, but not globally. Nature 488, 209–212.

Hirota, M., Holmgren, M., Van Nes, E.H., Scheffer, M., 2011. Global resilience of tropical forest and savanna to critical transitions. Science 334, 232–235.

Kéfi, S., Dakos, V., Scheffer, M., Van Nes, E.H., Rietkerk, M., 2013. Early warning signals also precede non-catastrophic transitions. Oikos 122, 641–648.

Kéfi, S., Rietkerk, M., Alados, C., Pueyo, Y., Papanastasis, V., ElAich, A., De Ruiter, P., 2007a. Spatial vegetation patterns and imminent desertification in Mediterranean arid ecosystems. Nature 449, 213–217.

Kéfi, S., Rietkerk, M., van Baalen, M., Loreau, M., 2007b. Local facilitation, bistability and transitions in arid ecosystems. Theor. Popul. Biol. 71, 367–379.

Kefi, S., Rietkerk, M., Katul, G., 2008. Vegetation pattern shift as a result of rising atmospheric CO_2 in arid ecosystems. Theor. Popul. Biol. 74, 332–344.

Klausmeier, C., 1999. Regular and irregular patterns in semiarid vegetation. Science 284, 1826–1828.

Konings, A., Katul, G., 2010. The rainfall–no rainfall transition in a coupled land-convective atmosphere system. Geophys. Res. Lett. 37 .

Konings, A.G., Dekker, S.C., Rietkerk, M., Katul, G.G., 2011. Drought sensitivity of patterned vegetation determined by rainfall-land surface feedbacks. J. Geophys. Res.: Biogeosci. 116, G04008.

Kröpelin, S., Verschuren, D., Lézine, A., Eggermont, H., Cocquyt, C., Francus, P., Cazet, J., Fagot, M., Rumes, B., Russell, J., et al., 2008. Climate-driven ecosystem succession in the Sahara: the past 6000 years. Science 320, 765–768.

Móréh, Á., Jordán, F., Szilágyi, A., Scheuring, I., 2009. Overfishing and regime shifts in minimal food web models. Commun. Ecol. 10, 236–243.

van Nes, E.H., Scheffer, M., 2007. Slow recovery from perturbations as a generic indicator of a nearby catastrophic shift. Am. Nat. 169, 738–747.

Pascual, M., Guichard, F., 2005. Criticality and disturbance in spatial ecological systems. Trends Ecol. Evol. 20, 88–95.

Perc, M., 2014. The Matthew effect in empirical data. J. R. Soc. Interface 11 .

Rietkerk, M., Boerlijst, M., van Langevelde, F., Hillerislambers, R., van de Koppel, J., Kumar, L., Prins, H., de Roos, A., 2002. Self-organization of vegetation in arid ecosystems. Am. Nat. 160, 524–530.

Rietkerk, M., Dekker, S.C., de Ruiter, P.C., van de Koppel, J., 2004. Self-organized patchiness and catastrophic shifts in ecosystems. Science 305, 1926–1929.

Rietkerk, M., Ketner, P., Burger, J., Hoorens, B., Olff, H., 2000. Multiscale soil and vegetation patchiness along a gradient of herbivore impact in a semi-arid grazing system in West Africa. Plant Ecol. 148, 207–224.

Rietkerk, M., van de Koppel, J., 2008. Regular pattern formation in real ecosystems. Trends Ecol. Evol. 23, 169–175.

Ripple, W.J., Beschta, R.L., 2006. Linking a cougar decline, trophic cascade, and catastrophic regime shift in Zion National Park. Biol. Conserv. 133, 397–408.

Sankaran, M., Hanan, N.P., Scholes, R.J., Ratnam, J., Augustine, D.J., Cade, B.S., Gignoux, J., Higgins, S.I., Le Roux, X., Ludwig, F., et al., 2005. Determinants of woody cover in African savannas. Nature 438, 846–849.

Scheffer, M., Bascompte, J., Brock, W.A., Brovkin, V., Carpenter, S.R., Dakos, V., Held, H., Van Nes, E.H., Rietkerk, M., Sugihara, G., 2009. Early-warning signals for critical transitions. Nature 461, 53–59.

Scheffer, M., Carpenter, S., Foley, J.A., Folke, C., Walker, B., 2001. Catastrophic shifts in ecosystems. Nature 413, 591–596.

Scheffer, M., Hirota, M., Holmgren, M., Van Nes, E.H., Chapin, F.S., 2012. Thresholds for boreal biome transitions. Proc. Natl. Acad. Sci. U. S. A. 109, 21384–21389.

Scheffer, M., Hosper, S., Meijer, M., Moss, B., Jeppesen, E., 1993. Alternative equilibria in shallow lakes. Trends Ecol. Evol. 8, 275–279.

Scheffer, M., Vergnon, R., Cornelissen, J.H.C., Hantson, S., Holmgren, M., van Nes, E.H., Xu, C., 2014. Why trees and shrubs but rarely trubs? Trends Ecol. Evol. 29, 433–434.

Seneviratne, S., Corti, T., Davin, E., Hirschi, M., Jaeger, E., Lehner, I., Orlowsky, B., Teuling, A., 2010. Investigating soil moisture–climate interactions in a changing climate: a review. Earth Sci. Rev. 99, 125–161.

Siteur, K., Eppinga, M.B., Karssenberg, D., Baudena, M., Bierkens, M.F., Rietkerk, M., 2014. How will increases in rainfall intensity affect semiarid ecosystems? Water Resour. Res. 50, 5980–6001.

Siteur, K., Siero, E., Eppinga, M.B., Rademacher, J.D.M., Doelman, A., Rietkerk, M., 2014b. Beyond turing: the response of patterned ecosystems to environmental change. Ecol. Complex. 20, 81–96.

Staver, A.C., Archibald, S., Levin, S., 2011a. Tree cover in sub-Saharan Africa: rainfall and fire constrain forest and savanna as alternative stable states. Ecology 92, 1063–1072.

Staver, A.C., Archibald, S., Levin, S.A., 2011b. The global extent and determinants of savanna and forest as alternative biome states. Science 334, 230–232.

Szolnoki, A., Mobilia, M., Jiang, L., Szczesny, B., Rucklidge, A.M., Perc, M., 2014. Cyclic dominance in evolutionary games: a review. J. R. Soc. Interface 11.

Tirabassi, G., Viebahn, J., Dakos, V., Dijkstra, H., Masoller, C., Rietkerk, M., Dekker, S., 2014. Interaction network based early-warning indicators of vegetation transitions. Ecol. Complex. 19, 148–157.

Turing, A., 1952. The chemical basis of morphogenesis. Philos. Trans. R. Soc. Lond. B: Biol. Sci. 237, 37–72.

Yin, Z., Dekker, S.C., van den Hurk, B.J.J.M., Dijkstra, H.A., 2014. Bimodality of woody cover and biomass across the precipitation gradient in West Africa. Earth Syst. Dyn. 5, 257–270.

Zeng, N., Yoon, J., 2009. Expansion of the world's deserts due to vegetation-albedo feedback under global warming. Geophys. Res. Lett. 36 .